Spin relaxometry of single nitrogen-vacancy defects in diamond nanocrystals for magnetic noise sensing

J.-P. Tetienne,[1,2] T. Hingant,[1,2] L. Rondin,[1] A. Cavaillès,[1] L. Mayer,[3] G. Dantelle,[3] T. Gacoin,[3] J. Wrachtrup,[4] J.-F. Roch,[2] and V. Jacques[1,2,*]

[1]*Laboratoire de Photonique Quantique et Moléculaire, CNRS and ENS Cachan UMR 8537, 94235 Cachan, France*

[2]*Laboratoire Aimé Cotton, CNRS, Université Paris-Sud and ENS Cachan, 91405 Orsay, France*

[3]*Laboratoire de Physique de la Matière Condensée, CNRS and Ecole Polytechnique UMR 7643, 91128 Palaiseau, France*

[4]*3. Physikalisches Institut and SCoPE, Universität Stuttgart, 70550 Stuttgart, Germany*

(Received 3 April 2013; published 27 June 2013)

We report an experimental study of the longitudinal relaxation time (T_1) of the electron spin associated with single nitrogen-vacancy (NV) defects hosted in nanodiamonds (NDs). We first show that T_1 decreases over three orders of magnitude when the ND size is reduced from 100 to 10 nm owing to the interaction of the NV electron spin with a bath of paramagnetic centers lying on the ND surface. We next tune the magnetic environment by decorating the ND surface with Gd^{3+} ions and observe an efficient T_1 quenching, which demonstrates magnetic noise sensing with a single electron spin. We estimate a sensitivity down to $\approx$14 electron spins detected within 10 s, using a single NV defect hosted in a 10-nm-size ND. These results pave the way towards T_1-based nanoscale imaging of the spin density in biological samples.

DOI: 10.1103/PhysRevB.87.235436 PACS number(s): 76.30.Mi, 07.55.Ge, 81.05.uj

The ability to detect spins is the cornerstone of magnetic resonance imaging (MRI), which is currently one of the most important tools in life science. However, the sensitivity of conventional MRI techniques is limited to large spin ensembles, which in turn restricts the spatial resolution at the micrometer scale.[1,2] Extending MRI techniques at the nanoscale can be achieved at a sub-Kelvin temperature with magnetic resonance force microscopy, through the detection of weak magnetic forces.[3,4] Another strategy consists in directly sensing the magnetic field created by spin magnetic moments with a nanoscale magnetometer. In that context, the electron spin associated with a nitrogen-vacancy (NV) defect in diamond has been recently proposed as an ultrasensitive and atomic-sized magnetic field sensor.[5] In the last years, many schemes based on dynamical decoupling pulse sequences have been devised for sensing AC or randomly fluctuating magnetic fields with a single NV spin.[6–9] These protocols recently enabled nuclear magnetic resonance measurements on a few cubic nanometers sample volume[10,11] and the detection of a single electron spin under ambient conditions.[12]

An alternative approach for sensing randomly fluctuating magnetic fields is based on the measurement of magnetic-noise-induced modifications of the longitudinal spin relaxation time (T_1) of the NV defect electron spin. This method does not require coherent manipulation of the NV defect with microwave pulses, which might be an important practical advantage for applications in biology. Using an ensemble of NV defects and a T_1-based sensing scheme, Steinert *et al.* recently demonstrated the detection of magnetic noise emanating from diffusing spins in a fluid, as well as imaging of spin-labeled cellular structures with a diffraction-limited spatial resolution ($\approx$500 nm).[13] Bringing the spatial resolution down to few nanometers could be achieved by using a single NV defect integrated in a scanning device, e.g., with a nanodiamond (ND) attached to the tip of an atomic force microscope (AFM).[14,15] With this application in mind, we study here the T_1 time of single NV defects hosted in NDs, as a function of ND size and magnetic environment. We first report a decrease of T_1 over three orders of magnitude when the ND size is reduced from 100 to 10 nm. This behavior is explained by considering the interaction of the NV spin with a bath of intrinsic paramagnetic centers lying on the ND surface. We next tune the magnetic environment by decorating the ND surface with paramagnetic molecules. As expected, a strong T_1 quenching is observed when the surface spin density is increased. From our data, we estimate a sensitivity of T_1-based relaxometry down to $\approx$14 electron spins detected within 10 s, using a single NV defect hosted in a 10 nm ND.

The NV defect ground state is a spin triplet ($S = 1$) with a zero-field splitting $D = 2.87$ GHz between a singlet state $m_s = 0$ and a doublet $m_s = \pm 1$ [Fig. 1(a)]. Owing to spin-dependent intersystem-crossing (ISC) towards intermediate singlet states, optical pumping leads to an efficient spin polarization into the $m_s = 0$ spin sublevel, while the spin state can be readout through spin-dependent photoluminescence (PL).[16] These two properties enable the measurement of the T_1 relaxation time of the NV defect electron spin by using the simple sequence depicted in the inset of Fig. 1(b). After initialization into the $m_s = 0$ spin sublevel with an optical pulse, the NV defect is kept in the dark for a time τ, causing the system to relax towards a mixture of states $m_s = 0, \pm 1$. The resulting electron spin state is read out by applying a second optical pulse. For a sufficiently short integration time (300 ns in this work), the readout PL signal $\mathcal{I}(\tau)$ can be written as $\mathcal{I}(\tau) \approx A_0 n_0(\tau) + A_1[n_{+1}(\tau) + n_{-1}(\tau)]$, where A_0 and $A_1 < A_0$ are the PL rates associated with spin states $m_s = 0$ and $m_s = \pm 1$, respectively, and $n_{0,\pm 1}(\tau)$ are the spin populations before applying the readout optical pulse. These populations are evaluated within the simplified four-level model shown in Fig. 1(a), which includes the ground-state spin sublevels $m_s = 0, \pm 1$ and the lowest-lying singlet state, thereafter referred to as the metastable state. We define T_1 as the decay time of the population n_0, hence $1/T_1 = 3k_{01}$, where k_{01} is the two-way transition rate between $m_s = 0$ and $m_s = \pm 1$.

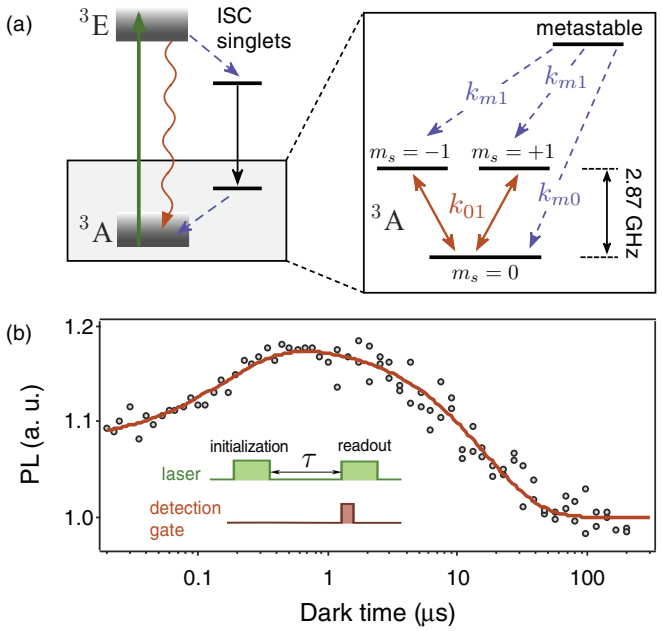

FIG. 1. (Color online) (a) Simplified energy-level structure of the NV defect. The zoom indicates the energy levels and transition rates used for studying the NV defect spin dynamics in the dark. (b) Integrated PL signal as a function of the dark time measured for a single NV center hosted in a 20 nm ND. The solid line is a fit to Eq. (1), which yields $T_1 = 16 \pm 1$ μs and $T_m = 160 \pm 30$ ns. The experimental sequence used to measure T_1 is shown in inset. Laser pulses with 3 μs duration are used both for initialization of the NV defect in $m_s = 0$ and for spin-state readout by recording the PL signal in a detection window corresponding to the first 300 ns of the optical pulses.

At short time scale, the spin populations are also affected by relaxation from the metastable state, which decays towards the ground state spin sublevels as $n_m(\tau) = n_m(0)e^{-\tau/T_m}$, where $T_m = (k_{m0} + 2k_{m1})^{-1}$ is the metastable state decay time. The value of this parameter is ≈200 ns.[16,17] Using classical rate equations within this four-level model, the PL signal $\mathcal{I}(\tau)$ can be written[18]

$$\mathcal{I}(\tau) = \mathcal{I}(\infty)[1 - C_m e^{-\tau/T_m} + C_1 e^{-\tau/T_1}]. \qquad (1)$$

The expressions of $\mathcal{I}(\infty)$, C_m, and C_1 are given in the Supplemental Material.[18] A typical measurement of $\mathcal{I}(\tau)$ is shown in Fig. 1(b) for a single NV defect hosted in a 20-nm-size ND, together with a fit to Eq. (1) yielding $T_1 = 16 \pm 1$ μs. This value is almost two orders of magnitude smaller than the one measured for single NV defects hosted in bulk diamond samples.[19]

To understand this behavior, the T_1 time was studied as a function of the ND size. We started from commercially available NDs (SYP 0.05 and 0.25, Van Moppes SA) produced by milling type-Ib high-pressure high-temperature (HPHT) diamond crystals with a high nitrogen content ([N] ≈ 200 ppm). The formation of NV defects was carried out using high-energy (13.6 MeV) electron irradiation followed by annealing at 800 °C under vacuum. The irradiated NDs were then oxidized in air at 550 °C over 2 h in order to remove graphitic-related defects on the surface and produce stable NV defects.[20] The NDs were finally spin cast on a glass cover slip and studied using a scanning confocal microscope combined with an AFM (Attocube Systems), all operating under ambient conditions.[18] For each photoluminescent ND, the PL intensity autocorrelation function was first recorded in order to verify that a single NV defect was hosted by the crystal. For a set of single NV defects in isolated NDs, the T_1 time was measured by fitting the relaxation curve $\mathcal{I}(\tau)$ to Eq. (1) and AFM measurements were used to infer the ND diameter d_0, defined as the maximum height in the AFM scan [Fig. 2(a)]. The relaxation rate $1/T_1$ is plotted as a function of the ND size in Fig. 2(b) for a set of 51 single NV defects in isolated NDs with d_0 ranging from 7 to 88 nm. An increase of the relaxation rate over three orders of magnitude is observed when the ND size decreases. Indeed, T_1 ranges from a few μs for the smallest (<10 nm) NDs to up to 1 ms for the biggest ones (>60 nm) [Figs. 2(a) and 2(b)].

For NV defects hosted in bulk diamond samples, phonon-assisted processes are the main causes of longitudinal spin relaxation at room temperature, with T_1 lying in the 1–10 ms range.[19] Relaxation induced by paramagnetic impurities like nitrogen atoms (P1 centers), which are the most abundant paramagnetic defects in type-Ib diamond, dominates only at low temperature and results in T_1 times that can be as long as 100 s at 4 K.[19] In NDs, a bath of paramagnetic centers covering the surface provides an additional channel for T_1 relaxation. These impurities have been identified by numerous studies[21–26] and are mainly ascribed to dangling bonds with unpaired electron spins. For NDs with an oxygen-terminated surface, as those used in this work, Tisler *et al.* determined a density of surface spins $\sigma \approx 1 - 10$ spin/nm^2 using spin coherence measurements and ensemble EPR measurements.[25] We attribute the shortening of T_1 of single NV spins in NDs to these surface paramagnetic centers (SPCs), which adds a contribution k_{01}^{spc} to the transition rate k_{01}^{bulk} of the bulk material, such that the overall rate is $k_{01} = k_{01}^{\text{bulk}} + k_{01}^{\text{spc}}$.

This hypothesis is tested by modeling the ND as a sphere and the SPCs as an ensemble of randomly fluctuating spins with a surface density σ [Fig. 2(c)]. The SPCs produce a fluctuating magnetic field $\mathbf{B}(t)$ with zero-mean $\langle B(t)\rangle = 0$, that is characterized by the spectral densities $S_{B_k}(\omega) = \int_{-\infty}^{+\infty} B_k(t)B_k(t+\tau)e^{-i\omega\tau}\mathrm{d}\tau$, where the three components $k = x, y, z$ are assumed to be uncorrelated. For a central NV spin $S = 1$ with an intrinsic quantization axis along z, one has[27]

$$k_{01}^{\text{spc}} = \frac{\gamma_e^2}{2}\left[S_{B_x}(\omega_0) + S_{B_y}(\omega_0)\right], \qquad (2)$$

where γ_e is the electron gyromagnetic ratio and $\omega_0 = 2\pi D$ is the electron spin resonance (ESR) frequency of the NV defect. As highlighted by Eq. (2), longitudinal spin relaxation is caused by the transverse components of the magnetic noise at the ESR frequency of the central spin. Assuming correlation functions of the form $\langle B_k(0)B_k(\tau)\rangle = \langle B_k^2\rangle e^{-|\tau|/\tau_c}$ where τ_c is the correlation time of the magnetic field and $\langle B_k^2\rangle$ its variance, the relaxation rate reads

$$\frac{1}{T_1} = \frac{1}{T_1^{\text{bulk}}} + 3\gamma_e^2 B_\perp^2 \frac{\tau_c}{1 + \omega_0^2\tau_c^2}. \qquad (3)$$

Here $B_\perp^2 = \langle B_x^2\rangle + \langle B_y^2\rangle$ is the variance of the transverse magnetic field, and $1/T_1^{\text{bulk}} = 3k_{01}^{\text{bulk}}$. Assuming $S = 1/2$

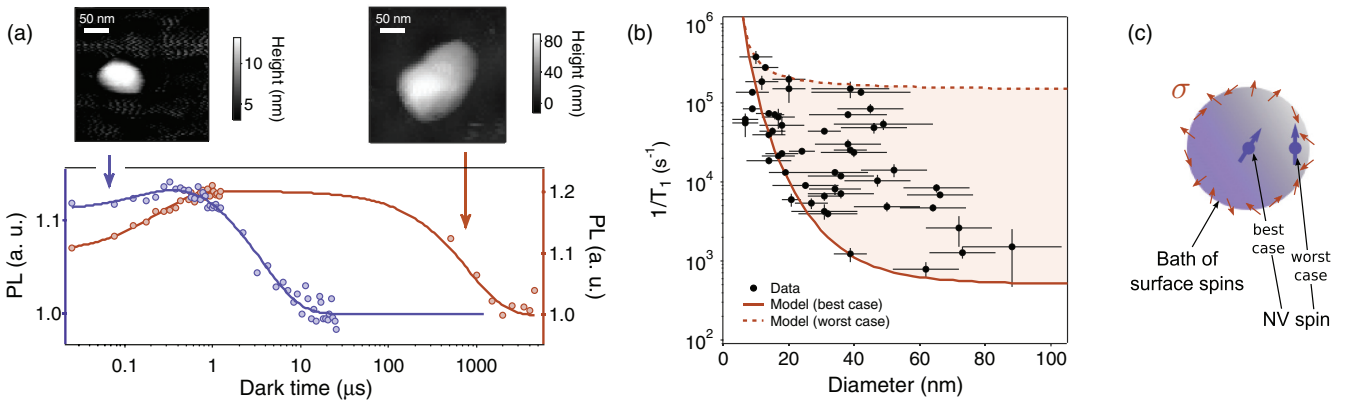

FIG. 2. (Color online) (a) Relaxation curves measured for a single NV defect hosted in a small ND ($d_0 = 13 \pm 3$ nm, blue curve) and a larger one ($d_0 = 73 \pm 10$ nm, red curve). Data fitting with Eq. (1) (solid lines) gives T_1 values of 3.6 ± 0.3 and 802 ± 136 μs, respectively. The corresponding AFM images are shown on top of the graph. (b) Longitudinal spin relaxation rate $1/T_1$ of the NV defect electron spin as a function of the ND diameter. We note that no obvious correlations with the size was observed for the other fitting parameters in Eq. (1), which were found to be $C_m = 0.084 \pm 0.037$, $C_1 = 0.21 \pm 0.12$, and $T_m = 198 \pm 72$ ns (mean $\pm$ s.d.). (c) The ND is modeled as a sphere with diameter d_0 with a bath of randomly fluctuating surface spins with density σ. In (b), the markers are experimental data while the lines are the results of the calculation using this model for a NV spin located at the center of the sphere (solid line) and 3 nm below the surface (dotted line). The parameters of the calculation are $T_1^{\text{bulk}} = 2$ ms and $\sigma = 1$ nm^{-2}.

surface spins, the variance $B_\perp^2$ is calculated by summing the dipolar field at the NV's location from each randomly oriented SPC and the correlation time τ_c is evaluated by considering intrabath dipolar coupling.[18] Since $B_\perp^2$ depends on the exact location and orientation of the NV defect inside the ND, the calculation is performed for two extreme configurations [Fig. 2(c)]. In the *best-case* scenario, the NV defect is located at the center of the sphere, while in the *worst-case* scenario, it is lying 3 nm below the surface, near the known photostability limit of the NV defect,[28] with its axis being parallel to the surface.[18] As shown in Fig. 2(b), the results of the model capture fairly well the experimental data with $\sigma = 1$ nm^{-2}. More precisely the relaxation rate scales as $1/d_0^4$ which stems from the $1/d_0^6$ dependence of the spin-spin interaction integrated over a surface.[29] This effect is responsible for the variation of T_1 over several orders of magnitude when the size of the ND decreases.[18]

In view of testing the ability of T_1 relaxometry to detect changes in the local magnetic environment, the ND surface was decorated with additional paramagnetic species. This was achieved by spin casting an aqueous solution of gadolinium perchlorate molecules $Gd(ClO_4)_3$, containing paramagnetic Gd^{3+} ions ($S = 7/2$), which is a well-known relaxation contrast agent in MRI. The T_1 time was measured for a set of 33 single NV defects in isolated NDs (1) before any treatment, (2) after a first treatment with 1 mM of Gd^{3+} solution, and (3) after a second treatment with 10 mM. The substrate was patterned with a metallic grid for precise and repeatable identification of each individual ND over repeated treatment steps. The histograms of the measured $1/T_1$ rates are shown in Fig. 3(a). The distribution is clearly shifted towards higher relaxation rate after each treatment step, which indicates that single NV defects feel the magnetic noise induced by the external Gd^{3+} ions. In Fig. 3(b) the relaxation rate after the first and second treatment step is plotted as a function of the rate in the bare nanocrystal, i.e., before any treatment. Almost all the investigated NV defects undergo a significant decrease in their T_1. The quenching ratio $\eta = T_{1,\text{bare}}/T_{1,\text{treated}}$ is found to be $\eta = 7$ on average after the first treatment with 1 mM of Gd^{3+} solution [Fig. 3(b)]. From this value, we estimate a surface density of Gd^{3+} spins $\sigma_{Gd} \approx 4$ nm^{-2}, corresponding to the detection of $\approx$1000 spins for a 10 nm ND.[18] After the second treatment step with 10 mM of Gd^{3+} solution, we obtain on average $\eta = 31$ corresponding to $\sigma_{Gd} \approx 70$ nm^{-2}. The dispersion in the measured values for η is attributed to a nonuniform surface spin density σ_{Gd}. In particular, NV defects located close to the diamond-substrate interface should be less affected by the Gd^{3+} treatment. It is worth mentioning that a similar environment-induced quenching effect could be observed on the spin coherence time T_2 as well, with however much smaller quenching ratios since $T_2^{\text{bulk}} \ll T_1^{\text{bulk}}$.[13,30] Furthermore, T_1-based sensing schemes do not require coherent manipulation of the NV electron spin with microwave pulses.

By applying a few more treatment steps with the Gd^{3+} solution, we then analyzed the regime of strongly fluctuating magnetic environment, bringing T_1 in the submicrosecond range. As shown in Fig. 4, T_1 quenching is accompanied by a significant reduction of the T_1 decay contrast, defined as $C_1^{\text{eff}} = \max[\mathcal{I}(\tau)]/\mathcal{I}(\infty) - 1$. In the inset of Fig. 4, we plot C_1^{eff} as a function of T_1 together with the calculation based on a rate equation model that takes into account the full dynamics of the NV defect.[18,31] The contrast reduction is mainly due to the overlap between T_m and T_1 decays [see Eq. (1)]. In addition, when $T_1 \sim T_m$, optical initialization in the $m_s = 0$ state and spin state readout become less efficient, thus reducing further the contrast.

Based on our experimental results, we finally estimate the sensitivity of T_1 relaxometry to small changes in the magnetic environment. For that purpose, we consider an optimized single-τ measurement by fixing $\tau \sim T_1/2$, which converts a modification of spin relaxation into a change of the PL signal $\mathcal{I}(\tau)$ with optimal signal-to-noise ratio.[13,18] Assuming

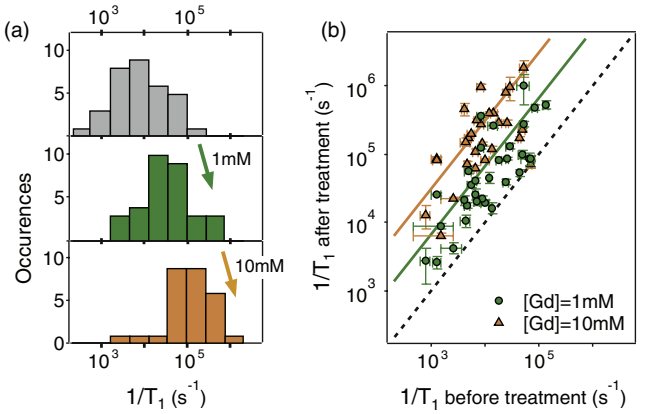

FIG. 3. (Color online) (a) Histograms of the $1/T_1$ relaxation rate obtained from a set of 33 single NV defects hosted in isolated NDs. The measurement is performed before any treatment (top panel), after adding 1 mM of the Gd^{3+} solution (middle panel) and after further adding 10 mM of solution (bottom panel). (b) Relaxation rate measured after the first (circles) and second (triangles) treatment step as a function of the rate of the bare ND. The solid lines are data fitting with linear functions whose slope indicates the average quenching ratio $\eta = T_{1,\mathrm{bare}}/T_{1,\mathrm{treated}}$. We obtain $\eta = 7$ (green line) and $\eta = 31$ (orange line). A dashed line of slope $\eta = 1$ is plotted for reference.

a photon shot noise limited signal, the smallest number of additional surface electronic spins $\delta\mathcal{N}_{\mathrm{min}}$ that can be detected by a single NV defect located at the center of a ND with size d_0 is given by

$$\delta\mathcal{N}_{\mathrm{min}} = \frac{1}{\mathcal{P}\sqrt{\Delta t}} d_0^4 f(\sigma), \tag{4}$$

where $\mathcal{P}$ includes both the finite contrast of the T_1 relaxation signal and the rate of detected photons, Δt is the integration time, and $f(\sigma)$ is a slowly increasing function of the intrinsic density of surface spins σ.[18] As expected, it is crucial to use NDs as small as possible in view of sensing magnetic noise from external spins. For a single NV defect hosted in a 10 nm ND with $\sigma = 1\,\mathrm{nm}^{-2}$, i.e., corresponding to $T_1 = 6.3\,\mu\mathrm{s}$ according to the above model [Fig. 2(b)], a typical photon counting rate $\mathcal{R} = 10^5\ \mathrm{s}^{-1}$ under CW optical illumination and a T_1 contrast $C_1 = 0.2$, we find $\delta\mathcal{N}_{\mathrm{min}} = 14$ spins within 10 s of integration.[32] This result highlights that T_1 relaxometry with a single NV spin hosted in a ND is a promising resource to probe nanoscale magnetic field fluctuations with a sensitivity down to a few electron spins, within a time scale that is compatible with scanning probe techniques. Such probes might find important applications in life sciences, e.g., to image the spin density in biological samples with an unprecedented spatial resolution.

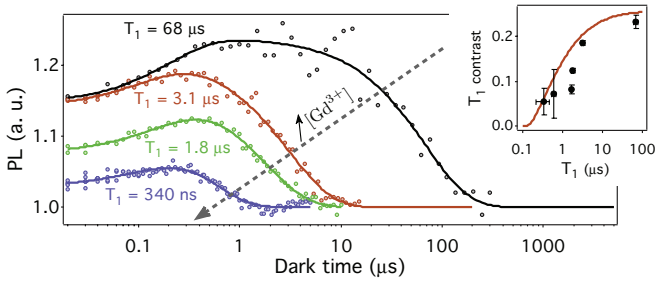

FIG. 4. (Color online) $\mathcal{I}(\tau)$ relaxation curves measured after repeated treatments with the Gd^{3+} solution. Solid lines are fit to Eq. (1). Inset: Effective T_1 contrast C_1^{eff} as a function of T_1. The solid line is the result of the calculation (with no fit parameter) using a rate equation model with the parameters of NV centers in bulk diamond.[18]

The authors thank J. Lautru, S. Steinert and F. Ziem for experimental assistance and fruitful discussions. This work was supported by C'Nano Ile-de-France and the ANR projects Diamag, Advice, and Qinvc.

*vjacques@ens-cachan.fr

[1] S.-C. Lee, K. Kima, J. Kim, S. Lee, J. H. Yi, S. W. Kim, K.-S. Ha, and C. Cheong, J. Magn. Reson. **150**, 207 (2001).
[2] L. Ciobanu, D. A. Seeber, and C. H. Pennington, J. Magn. Reson. **158**, 178 (2002).
[3] H. J. Mamin, M. Poggio, C. L. Degen, and D. Rugar, Nat. Nanotech. **2**, 301 (2007).
[4] C. L. Degen, M. Poggio, H. J. Mamin, C. T. Rettner, and D. Rugar, Proc. Natl. Acad. Sci. USA **106**, 1313 (2009).
[5] J. M. Taylor, P. Cappellaro, L. Childress, L. Jiang, D. Budker, P. R. Hemmer, A. Yacobi, R. Walsworth, and M. D. Lukin, Nat. Phys. **4**, 810 (2008).
[6] J. R. Maze *et al.*, Nature (London) **455**, 644 (2008).
[7] L. T. Hall, J. H. Cole, C. D. Hill, and L. C. L. Hollenberg, Phys. Rev. Lett. **103**, 220802 (2009).
[8] A. Laraoui, J. S. Hodges, and C. A. Meriles, Appl. Phys. Lett. **97**, 143104 (2010).
[9] G. de Lange, D. Ristè, V. V. Dobrovitski, and R. Hanson, Phys. Rev. Lett. **106**, 080802 (2011).
[10] H. J. Mamin, M. Kim, M. H. Sherwood, C. T. Rettner, K. Ohno, D. D. Awschalom, and D. Rugar, Science **339**, 557 (2013).
[11] T. Staudacher, F. Shi, S. Pezzagna, J. Meijer, J. Du, C. A. Meriles, F. Reinhard, and J. Wrachtrup, Science **339**, 561 (2013).
[12] M. S. Grinolds, S. Hong, P. Maletinsky, L. Luan, M. D. Lukin, R. L. Walsworth, and A. Yacoby, Nat. Phys. **9**, 215 (2013).
[13] S. Steinert, F. Ziem, L. Hall, A. Zappe, M. Schweikert, A. Aird, G. Balasubramanian, L. Hollenberg, and J. Wrachtrup, Nat. Comm. **4**, 1607 (2013).
[14] G. Balasubramanian *et al.*, Nature (London) **455**, 648 (2008).
[15] L. Rondin, J.-P. Tetienne, P. Spinicelli, C. Dal Savio, K. Karrai, G. Dantelle, A. Thiaville, S. Rohart, J.-F. Roch, and V. Jacques, Appl. Phys. Lett. **100**, 153118 (2012).
[16] N. B. Manson, J. P. Harrison, and M. J. Sellars, Phys. Rev. B **74**, 104303 (2006).
[17] L. Robledo, H. Bernien, T. van der Sar, and R. Hanson, New J. Phys. **13**, 025013 (2011).
[18] See Supplemental Material at http://link.aps.org/supplemental/10.1103/PhysRevB.87.235436 for details.

[19] A. Jarmola, V. M. Acosta, K. Jensen, S. Chemerisov, and D. Budker, Phys. Rev. Lett. **108**, 197601 (2012).
[20] L. Rondin, G. Dantelle, A. Slablab, F. Grosshans, F. Treussart, P. Bergonzo, S. Perruchas, T. Gacoin, M. Chaigneau, H.-C. Chang, V. Jacques, and J.-F. Roch, Phys. Rev. B **82**, 115449 (2010).
[21] A. I. Shames *et al.*, J. Phys. Chem. Solids **63**, 1993 (2002).
[22] M. Dubois, K. Guering, E. Petit, N. Batisse, A. Hamwi, N. Komatsu, J. Giraudet, P. Pirotte, and F. J. Masin, Phys. Chem. C **113**, 10371 (2009).
[23] L. B. Casabianca, A. I. Shames, A. M. Panich, O. Shenderova, and L. J. Frydman, Phys. Chem. C **115**, 19041 (2011).
[24] A. M. Panich and G. B. Furman, Diamond Relat. Mater. **23**, 157 (2012).
[25] J. Tisler *et al.*, ACS Nano **3**, 1959 (2009).
[26] A. Laraoui, J. S. Hodges, and C. A. Meriles, Nano Lett. **12**, 3477 (2012).
[27] C. P. Slichter, *Principles of Magnetic Resonance* (Springer, New York, 1990).
[28] C. Bradac, T. Gaebel, N. Naidoo, M. J. Sellars, J. Twamley, L. J. Brown, A. S. Barnard, T. Plakhotnik, A. V. Zvyagin, and J. R. Rabeau, Nat. Nanotech. **5**, 345 (2010).
[29] In contrast with NV defects in bulk diamond, T_1 could thus not be increased by lowering the temperature.
[30] L. P. McGuinness *et al.*, arXiv:1211.5749.
[31] J.-P. Tetienne, L. Rondin, P. Spinicelli, M. Chipaux, T. Debuisschert, J.-F. Roch, and V. Jacques, New J. Phys. **14**, 103033 (2012).
[32] For this calculation, we have $\mathcal{P} = 179\ \mathrm{s}^{-1/2}\ \mathrm{nm}^{5/2}$, $f(\sigma = 1\ \mathrm{nm}^{-2}) = 0.78\ \mathrm{nm}^{-3/2}$, and $f(\sigma)/\mathcal{P} = 0.0043\ \mathrm{s}^{1/2}\ \mathrm{nm}^{-4}$.[18]